Available online at www.sciencedirect.com
SCIENCE DIRECT®
Surface Science 584 (2005) 153–160
SURFACE SCIENCE
www.elsevier.com/locate/susc

Growth of thin platinum films on Cu(1 0 0): CAICISS, XPS and LEED studies

M. Walker, C.R. Parkinson, M. Draxler, C.F. McConville *

Department of Physics, University of Warwick, Coventry CV4 7AL, UK

Received 9 November 2004; accepted for publication 24 March 2005
Available online 13 April 2005

Abstract

The growth mode of platinum films on the Cu(1 0 0) surface up to a coverage of 2.75 ML has been studied using co-axial impact collision ion scattering spectroscopy (CAICISS), X-ray photoelectron spectroscopy and low energy electron diffraction. CAICISS data show the formation of a Cu–Pt alloy at room temperature in the top three atomic layers at sub-monolayer Pt coverage. As the coverage increases up to 2.75 ML the formation of a Pt overlayer is observed in conjunction with the near surface region becoming Pt-rich, indicating the onset of layer-by-layer growth. Subsequent annealing shows a significant migration of Pt into the bulk Cu at a temperature of 300 °C. Evidence for a more ordered surface after annealing is also presented.

Keywords: Low energy ion scattering (LEIS); Low energy electron diffraction (LEED); X-ray photoelectron spectroscopy; Platinum; Copper; Alloys

1. Introduction

Alloys and bimetallic surfaces have received much attention in recent years due to their importance in many modern technological processes (e.g. heterogeneous catalysis and magnetic recording [1–3]). The deposition of one metal on a substrate of a second metallic species (e.g. Pt on Cu(1 0 0)) allows production of alloys with controllable concentrations, and may present surfaces with different characteristics to those of single crystal alloy surfaces (e.g. Cu_xPt_y(1 0 0)).

The Cu–Pt surface alloy system has been the subject of numerous studies, ranging from Cu deposition on Pt surfaces [4–7], to single crystal alloy surfaces [8,9] and Pt deposition on Cu surfaces [10–25]. The formation of Cu–Pt alloys on the Cu(1 1 1) surface by Pt deposition and subsequent annealing has been widely studied using many

* Corresponding author. Tel.: +44 24 7652 4236; fax: +44 24 7669 2016.
E-mail address: c.f.mcconville@warwick.ac.uk (C.F. McConville).

0039-6028/$ - see front matter
doi:10.1016/j.susc.2005.03.050

experimental and theoretical techniques [10–20]. However, similar investigations on Cu(1 0 0) have been less common [21–25], and hence the characteristics of this system are less well understood.

One of the earliest studies of the Cu(1 0 0)/Pt alloy was carried out by Graham et al. using Auger electron spectroscopy (AES), low energy ion scattering (LEIS) and low energy electron diffraction (LEED) [21]. In this study it was demonstrated that at room temperature, Pt forms disordered islands on the surface with some intermixing from the Cu substrate, giving a weak c(2 × 2) LEED pattern which strengthened significantly on annealing to 300 °C. This ordering was attributed to the formation of a pure Cu surface layer with a Cu–Pt alloy formed beneath the surface. A tensor low energy electron diffraction (TLEED) study by Al Shamaileh et al. supported this analysis by observing pure Cu surface layers after annealing samples with Pt coverages of 0.5 ML, 1.0 ML and 1.5 ML at 300 °C [24]. This view was also shared by Reilly et al. who observed a c(2 × 2) structure after annealing to 230 °C [23].

Belkhou et al. used photoemission spectroscopy (PES) and LEED to look at Pt deposition on Cu(1 0 0) up to a coverage of 2 ML [22]. They observed the formation of an extended surface alloy during growth with the Pt concentration in the top layer being approximately 50%, which is consistent with the c(2 × 2) LEED patterns reported. They also showed that at higher coverages the alloy was destroyed and a disordered pure Pt film started to grow. Annealing of the Pt film led to the reformation of the Cu–Pt extended surface alloy.

In this paper, the growth mode of Pt thin films up to a coverage of 2.75 ML and the effects of subsequent annealing have been studied by co-axial impact collision ion scattering spectroscopy (CAICISS). CAICISS is a unique surface science technique which offers both chemical and structural information with a high degree of surface specificity. Recently this technique has been used for investigations of many adsorbate–substrate systems [27–29]. The technique relies on the fact that the scattering of inert gas ions at relatively low energies (2–5 keV) from a surface can be described in terms of a simple binary collision model [30]. Analysis of the energy and flux of the scattered ions and neutral particles, as a function of incidence or azimuthal angle, offers the possibility to construct the chemical composition and atomic structure of the surface with single-layer sensitivity. In addition, LEED has been used to monitor the surface periodicity, whilst X-ray photoelectron spectroscopy (XPS) was used to support the alloy compositions determined by CAICISS and to check for any surface contamination.

2. Experimental detail

The experiments were carried out in a UHV chamber equipped with a retractable LEED optic (Omicron GmbH, Germany), a dual anode X-ray source (Vacuum Generators, UK), a 100 mm concentric hemispherical electron energy analyser (VSW, UK, HA100), and a modular CAICISS system. The main chamber is pumped by ion and diffusion pumps, and has a nominal base pressure in the 10^{-10} mbar regime. The Cu(1 0 0) crystal (Metal Crystals and Oxides, UK), cut to ±0.1° of the (1 0 0) plane, was mechanically polished and etched before being mounted on the end of a manipulator capable of polar and azimuthal rotation. Resistive sample heating to 800 °C was monitored using a chromel–alumel thermocouple in contact with the sample. XPS spectra were taken using the MgK_α anode of the X-ray source ($h\nu$ = 1253.6 eV), with all binding energies calibrated relative to the Cu $2p_{3/2}$ peak at 932.8 eV [26].

2.1. Sample preparation

The Cu(1 0 0) crystal was cleaned using cycles of Ar^+ bombardment at 3 keV and extended annealing at 800 °C. Typically, two or three cycles were required until no impurities were observed in the XPS spectrum of the surface. The clean surface exhibited a sharp (1 × 1) LEED pattern (see inset of Fig. 2). Deposition of Pt was achieved using a metal evaporation source consisting of a high purity Pt wire wound around a tungsten filament, with a current of 14.5 A passing through the filament. Pt deposition was carried out at pressures of less than 1×10^{-8} mbar. The W 4d, C 1s and O 1s photoemission peaks were monitored to ensure that the surfaces were free from contamination both prior to and following deposition.

2.2. CAICISS

A schematic of the modular CAICISS instrument used for this investigation is shown in Fig. 1, and is described in detail elsewhere [29]. All of the data presented in this paper were collected using a 3 keV He^+ ion beam produced from research grade helium (Air Products, UK). Data acquisition was carried out using an EG&G Ortec multichannel buffer (MCB) with dedicated software.

The scattering geometry and the axes defining the incidence (polar) angle, α, and azimuthal angle, ϕ, are shown in the upper-right quadrant of Fig. 1. Note that α is defined relative to the surface plane, so in changing this angle from 0° to 180°, the scattering geometry passes from grazing incidence, through to normal incidence (90°) and back to grazing incidence from the opposite edge of the crystal. This data acquisition mode (polar scan) has been automated using a stepper motor, allowing data to be collected in 1.8° steps. For this investigation, an acquisition time of 100 s was employed at each step.

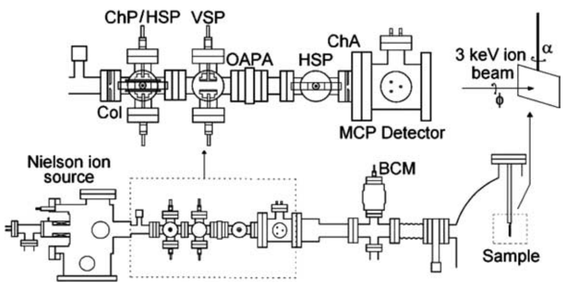

Fig. 1. Schematic diagram of the Warwick CAICISS apparatus, explained in detail elsewhere [29]. Several components are labelled in the central section of the ion column (upper image): MCP, micro-channel plate detector; OAPA, off-axis port aligner; ChP, chopping plates; ChA, chopping aperture; BCM, beam current monitor; HSP and VSP, horizontal and vertical steering plates; Col, collimating aperture. The axes defining the polar angle, α, and azimuthal angle, ϕ, are shown in the upper-right quadrant.

2.3. XPS and CAICISS data analysis

Structural information has been obtained from CAICISS spectra by measuring the Cu and Pt backscattered intensity as a function of polar angle after each Pt deposition and anneal treatment. A combination of CAICISS data, LEED and XPS was used to determine the Pt coverage in each case.

To enable accurate interpretation of the CAICISS data, the FAN simulation software developed by Niehus [32] has been used to determine the atomic structure and composition of the five outmost atomic layers. This package allowed quantitative structural analysis, concentrating on the relative intensities of the peaks within the spectrum and the angular position of the peaks relative to the experimental data. Many iterations were performed (typically around 20 to 30 for each data set), modifying the layer-by-layer composition, the interlayer spacings and the interatomic spacings until an acceptable fit was obtained.

XPS data analysis was used to determine the total amount of Pt deposited on to the Cu(100) surface. Fitting involved the employment of a Gaussian–Lorentzian mixture (70%:30%) to determine the area of the Cu $2p_{3/2}$ peak prior to Pt deposition, as well as the Pt $4f_{7/2}$ and Cu $2p_{3/2}$ peaks following each deposition stage. Quantification methods outlined by Carley and Roberts [31] were then used to estimate the Pt surface concentration and total coverage.

3. Results and discussion

3.1. The clean Cu(100) surface

CAICISS data from the clean Cu(100) surface in the $\langle 100 \rangle$ azimuth is shown in Fig. 2 along with the FAN simulation results for the trial structure with the best fit in terms of peak positions. With reference to Fig. 2, the peak at approximately 16° corresponds to surface layer scattering, the peak at 45° corresponds to second atomic layer scattering, whilst the peaks at 68° and 78° correspond to scattering from deeper layers. Similarly, experimental data and simulation results in the $\langle 110 \rangle$ azimuth are shown in Fig. 3. The trial

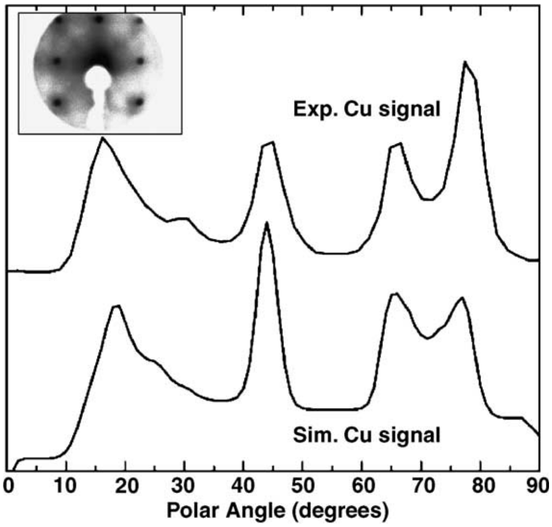

Fig. 2. CAICISS peak profile from the clean Cu(1 0 0) surface in the ⟨1 0 0⟩ azimuth and the FAN simulation results. The inset in the upper-left shows the inverse of the (1×1) LEED pattern recorded from the surface at an energy of 120 eV.

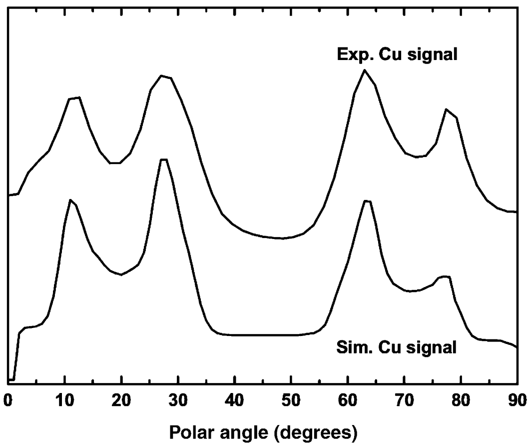

Fig. 3. CAICISS peak profile from the clean Cu(1 0 0) surface in the ⟨1 1 0⟩ azimuth and the corresponding FAN simulation.

structure with the best fit in both azimuths exhibited a 1.6% contraction in the outermost interlayer spacing, Δ_{12}, to 1.78 Å, relative to the bulk Cu(1 0 0) value of 1.81 Å. The second interlayer spacing, Δ_{23}, was determined to be 1.84 Å, a 1.6% expansion relative to the bulk interlayer spacing. The interlayer spacing in deeper layers reverts back to the bulk value of 1.81 Å. This model gave a good quantitative fit and agrees with previous reports on the structure of the clean Cu(1 0 0) surface [33]. The results from the clean surface, as well as trial simulations for the various different growth modes of Pt on Cu(1 0 0), indicated that data taken in the ⟨1 0 0⟩ azimuth would provide all the necessary information to determine the growth mode and layer-by-layer composition.

3.2. Deposition and annealing of Pt on Cu(1 0 0)

3.2.1. LEED and XPS observations

Diffraction patterns were observed after each Pt deposition (with coverages of 0.55 ML, 1.00 ML, 2.35 ML and 2.75 ML, as determined by XPS), and upon annealing for 10 min at 200 °C and 300 °C. The clean Cu(1 0 0) surface exhibited a sharp (1×1) reconstruction. Following the first Pt deposition ($\theta_{Pt} \simeq 0.55$ ML), the surface exhibited a weak $c(2 \times 2)$ LEED pattern as reported previously [22,23]. This pattern is characteristic of a poorly-ordered alloy in the surface region. The $c(2 \times 2)$ LEED pattern became progressively weaker, with higher background intensity, as the Pt coverage was increased. No diffraction spots were visible at a coverage of 2.75 ML. No diffraction pattern was observed upon annealing at 200 °C, suggesting that the disorder in the surface region is not removed by brief annealing treatments at relatively low temperatures. However a weak $c(2 \times 2)$ pattern was observed upon annealing at 300 °C, indicating some degree of ordering in the alloy structure.

Fig. 4 shows the Cu 3p and Pt 4f XPS spectra taken at each stage of the Pt deposition process, as well as the subsequent annealing of the sample with a Pt concentration of 2.75 ML. Here we observe the disappearance of the Cu 3p peak with increasing Pt coverage, indicating that the surface is Pt-rich. Following annealing at 300 °C the intensity of the Pt 4f peaks decreased, indicating diffusion of some Pt away from the surface region.

3.2.2. CAICISS observations

A summary of layer-by-layer compositions, interlayer spacings and observed LEED patterns are given in Table 1. The Pt peak in the CAICISS data as a function of polar (incidence) angle for

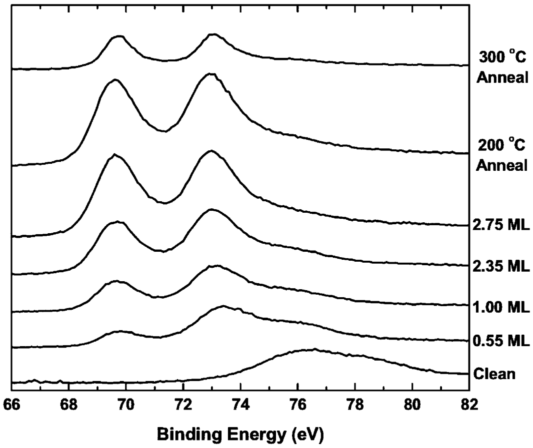

Fig. 4. The Pt 4f (69.8 eV, 73.1 eV) and Cu 3p (76.6 eV) photoemission peaks from clean Cu(1 0 0), Pt deposition up to a coverage of 2.75 ML and subsequent annealing.

the surface following deposition of 0.55 ML of Pt is shown in Fig. 5, together with simulations for three possible Pt growth modes (layer-by-layer growth, Pt clusters on the surface and an alloy in the top three layers of the Cu(1 0 0) crystal). The features at incidence angles of approximately 17°, 45°, 68° and 78° are most accurately reproduced by the model containing Pt in the three outermost layers of the crystal. This model is unique in predicting the small peak at approximately 32°, and also most accurately predicts the surface peak at 17°. The proposed model structure is detailed in Table 1.

The Cu–Pt alloy formation continues with the central peaks in the CAICISS spectra becoming more pronounced with increasing Pt deposition up to 2.75 ML, as shown in Fig. 6. The proposed structures are summarized in Table 1. Of particular interest is the change in the structure of the alloy with increasing Pt coverage. In the 1.00 ML case, a substitutional alloy was formed with the surface layer containing ∼80% Pt. The remaining 20% of the Pt penetrated into the second and third layers. In the 2.35 ML case, the concentrations were found to be 87% Pt in the surface layer, 85% Pt in the second layer and 50% Pt in the third layer. We notice here that a small peak appeared at an incidence angle of 32°. This feature could only be explained by a small coverage (∼0.12 ML) of Pt sitting 2.2 Å above the outermost complete atomic layer, indicating the possible onset of layer-by-layer growth. Increasing the Pt coverage to 2.75 ML saw the 0.12 ML Pt overlayer remain unchanged, whilst the Pt concentrations in the surface layer and the second atomic layer changed to 100% and 90%, respectively. An increase in the amount of Pt in layers 3, 4 and 5 was also observed.

Table 1
LEED patterns, XPS data and results of FAN simulations of CAICISS data for Pt deposition up to 2.75 ML and subsequent annealing at 200 °C and 300 °C

Total Pt coverage (ML)	0.00	0.55	1.00	2.35	2.75	200 °C anneal	300 °C anneal
LEED pattern	(1 × 1)	c(2 × 2)	Streaky c(2 × 2)	Weak c(2 × 2)	None	None	Weak c(2 × 2)
Pt overlayer (ML)	–	0	0	0.12	0.12	0.12	0.05
Surface layer Pt %	–	45	80	87	100	100	50
Layer 2 Pt %	–	5	10	85	90	90	33
Layer 3 Pt %	–	5	10	50	55	55	25
Layer 4 Pt %	–	0	0	0	5	5	25
Layer 5 Pt %	–	0	0	0	15	15	25
Overlayer to surface distance (Å)	–	–	–	2.20	2.20	2.20	2.20
Δ_{12} (Å)	1.78	2.00	2.00	1.90	2.00	2.00	2.00
Δ_{23} (Å)	1.84	1.85	1.81	1.81	1.81	1.81	1.81
Δ_{34} (Å)	1.81	1.81	1.81	1.81	1.81	1.81	1.81
Δ_{45} (Å)	1.81	1.81	1.81	1.81	1.81	1.81	1.81

The total Pt coverages determined by XPS are accurate to ±0.05 ML. The individual layer compositions were determined by CAICISS simulations and are accurate to ±5%.

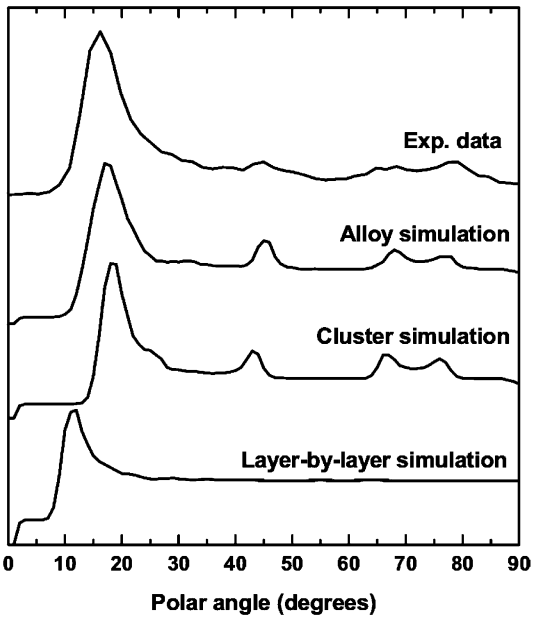

Fig. 5. Experimental Pt peak profile from Cu(1 0 0) with a Pt coverage of 0.55 ML and simulations of three possible growth models (layer-by-layer, Pt clusters on the surface, and a Cu–Pt alloy in the top three layers of the crystal). The experimental data are well reproduced by the three-layer Cu–Pt alloy model.

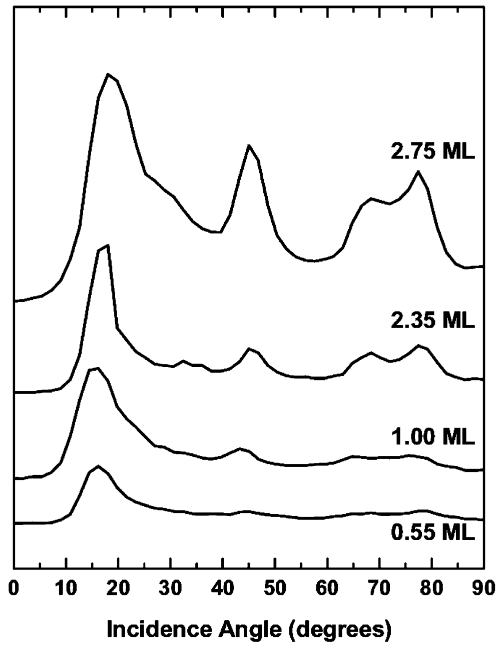

Fig. 6. CAICISS Pt peak profile as a function of Pt coverage. Peaks corresponding to sub-surface Pt are present at sub-monolayer coverage suggesting the formation of an alloy on deposition. These peaks increase in intensity with further Pt deposition up to 2.75 ML.

We also note that during the growth process the surface peak and second layer peak both shifted to higher polar angles. The surface peak recorded at 16° on the clean surface was shifted to 18° after Pt deposition of 2.75 ML. The peak corresponding to scattering from second layer atoms shifted in a similar manner from 44° to 45°. This indicates a change in interlayer spacing Δ_{12} during the deposition process as the larger Pt atoms are accommodated within the alloy structure.

Annealing the highest Pt coverage (2.75 ML) to 200 °C yielded a negligible change in the CAICISS spectrum. Previous studies have suggested that significant diffusion of Pt atoms into the Cu(1 0 0) substrate begins at temperatures around 300 °C [22,24,25]. The Pt CAICISS profile, before and after annealing to 300 °C, is shown in Fig. 7. The data clearly showed an increase in the intensity of the sub-surface scattering peaks (at 65° and 78°) relative to the surface peak (at 18°). From this we deduce that significant amounts of Pt migrated from the surface layer (100% Pt prior to annealing), second layer (90% Pt prior to annealing) and third layer (50% Pt prior to annealing) to deeper layers (i.e. the 4th and 5th layers). It should also be noted that the peaks have become sharper, indicating some ordering in the alloy structure. This is in agreement with the observation of a weak c(2 × 2) LEED pattern.

Simulation results, shown in Table 1, suggest the formation of a CuPt alloy at the surface, with a 0.05 ML Pt overlayer sitting 2.2 Å above the surface. A Cu_2Pt alloy was formed in the second layer, 2.0 Å below the surface. Deeper into the sample, the third, fourth and fifth layers became a Cu_3Pt alloy as suggested in previous studies [22,24], with interlayer spacings moving back towards bulk Cu(1 0 0) values. Due to the large shadow cone widths (~1.4 Å) resulting from the low energy ions used in CAICISS [30], we could not penetrate deeper than five layers into the sample. Annealing to 600 °C led to the loss of Pt from the CAICISS spectrum.

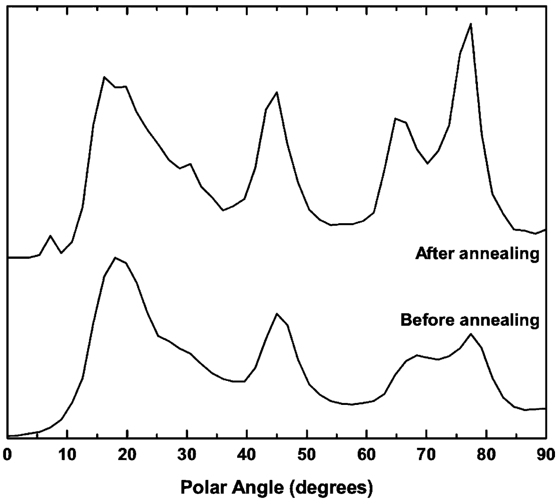

Fig. 7. CAICISS Pt peak profiles before and after 300 °C annealing treatment, normalised to the backscattered Pt intensity at 17°. The visible increase of the intensity of the subsurface Pt peaks indicated the migration of Pt from the surface into the substrate. The sharpening of the features in the spectrum gives evidence that some ordering has occurred within the alloy structure. The small peak at 8° in the annealed data is due to the ion beam striking Ta clips used to hold the sample.

4. Summary

In this paper we have presented evidence for changes in the interlayer spacings in the surface region of clean Cu(100) relative to the bulk structure. We have also presented evidence for the formation of Cu–Pt alloys at Pt coverages ranging from 0.55 ML to 2.75 ML, deducing the layer-by-layer composition and interlayer spacings after each Pt deposition. At higher coverages the surface becomes Pt-rich. Moreover, certain features observed in the CAICISS data at higher Pt coverages can only be explained by a small Pt concentration (0.12 ML) on top of the Pt-rich surface layers. This indicates the onset of layer-by-layer growth of a pure Pt film. Annealing of the sample containing 2.75 ML of Pt at 300 °C resulted in the migration of Pt from the surface region into the substrate and forming a more ordered alloy structure. The annealing yielded a CuPt alloy surface layer, a Cu_2Pt alloy in the second layer and a Cu_3Pt alloy in deeper layers of the crystal. Some ordering is indicated by the sharpening of the peaks in the CAICISS data and by the weak c(2 × 2) LEED pattern observed.

Acknowledgments

Rob Johnston is thanked for technical support during this investigation. M. Walker thanks the EPSRC for a DTA Studentship. M. Draxler acknowledges the support of the Austrian Science Fund (FWF) via an Erwin Schrödinger Fellowship (project number J2417-N08).

References

[1] P. Beccat, J.C. Bertolini, Y. Gauthier, J. Massardier, P. Ruiz, J. Catal. 126 (1990) 451.
[2] C.-J. Lin, G.L. Gorman, C.H. Lee, R.F.C. Farrow, E.E. Marinero, H.V. Do, H. Notarys, C.J. Chien, J. Magn. Magn. Mater. 93 (1991) 194.
[3] W.B. Zeper, H.W. van Kesteren, B.A.J. Jacobs, J.H.M. Spruit, P.F. Carcia, J. Appl. Phys. 70 (1991) 2264.
[4] J. Radnik, B.D. Wagner, K. Oster, K. Wandelt, Surf. Sci. 357–358 (1996) 943.
[5] N.M. Markovic, B.N. Grgur, C.A. Lucas, P.N. Ross, Electrochim. Acta 44 (1998) 1009.
[6] J.S. Tsay, T. Mangen, K. Wandelt, Thin Solid Films 397 (2001) 152.
[7] J.S. Tsay, T. Mangen, R.-J. Linden, K. Wandelt, Surf. Sci. 482–485 (2001) 866.
[8] Y.G. Shen, D.J. O'Connor, K. Wandelt, R.J. MacDonald, Surf. Sci. 328 (1995) 21.
[9] Y.G. Shen, D.J. O'Connor, K. Wandelt, Surf. Sci. 410 (1998) 1.
[10] R. Belkhou, N.T. Barrett, C. Guillot, A. Barbier, J. Eugne, B. Carrire, D. Naumovic, J. Osterwalder, Appl. Surf. Sci. 65–66 (1993) 63.
[11] R. Belkhou, N.T. Barrett, C. Guillot, M. Fang, A. Barbier, J. Eugne, B. Carrire, D. Naumovic, J. Osterwalder, Surf. Sci. 297 (1993) 40.
[12] N.T. Barrett, R. Belkhou, J. Thiele, C. Guillot, Surf. Sci. 331–333 (1995) 776.
[13] J. Fusy, J. Menaucourt, M. Alnot, C. Huguet, J.J. Ehrhardt, Appl. Surf. Sci. 93 (1996) 211.
[14] Y.G. Shen, D.J. O'Connor, B.V. King, R.J. MacDonald, Nucl. Instrum. Meth. B 115 (1996) 191.
[15] U. Schröder, R. Linke, J.-H. Boo, K. Wandelt, Surf. Sci. 352–354 (1996) 211.
[16] U. Schröder, R. Linke, J.-H. Boo, K. Wandelt, Surf. Sci. 357–358 (1996) 873.
[17] Y.G. Shen, D.J. O'Connor, K. Wandelt, R.J. MacDonald, Surf. Sci. 357–358 (1996) 921.
[18] A. Christensen, A.V. Ruban, P. Stoltze, K.W. Jacobsen, H.L. Skriver, J.K. Nørskov, F. Besenbacher, Phys. Rev. B 56 (1997) 5822.

[19] Y.G. Shen, D.J. O'Connor, K. Wandelt, Nucl. Instrum. Meth. B 135 (1998) 361.
[20] J.-H. Boo, S.-Y. Lee, S.-B. Lee, H.-T. Kwak, U. Schröder, R. Linke, K. Wandelt, J. Korean Phys. Soc. 35 (1999) S554.
[21] G.W. Graham, P.J. Schmitz, P.A. Thiel, Phys. Rev. B 41 (1990) 3353.
[22] R. Belkhou, J. Thiele, C. Guillot, Surf. Sci. 377–379 (1997) 948.
[23] J.P. Reilly, D. O'Connell, C.J. Barnes, J. Phys.: Condens. Matter 11 (1999) 8417.
[24] E. Al Shamaileh, H. Younis, C.J. Barnes, K. Pussi, M. Lindroos, Surf. Sci. 515 (2002) 94.
[25] G. Demarco, J.E. Garcés, G. Bozzolo, Surf. Sci. 526 (2003) 309.
[26] J. Chastain, R.C. King Jr. (Eds.), Handbook of X-ray Photoelectron Spectroscopy, Physical Electronics, Eden Prairie, 1995.
[27] J. Yuhara, K. Matsuda, Y. Hattori, K. Morita, Appl. Surf. Sci. 162–163 (2000) 368.
[28] H. Niehus, M. Voetz, C. Achete, K. Morgenstern, G. Cosma, in: R.J. MacDonald, E. Taglauer, K. Wandelt (Eds.), Surface Science, Principles and Current Applications, Springer, 1996, p. 38.
[29] C.R. Parkinson, M. Walker, C.F. McConville, Surf. Sci. 545 (2003) 19.
[30] H. Niehus, W. Heiland, E. Taglauer, Surf. Sci. Rep. 17 (1993) 213.
[31] A.F. Carley, M.W. Roberts, Proc. R. Soc. London A 363 (1978) 403.
[32] H. Niehus, FAN Simulation Software, Humboldt-Universität zu Berlin, Institut für Physik, Berlin. Available from: <http://asp2.physik.hu-berlin.de/>.
[33] T.D. Pope, et al., Surf. Sci. 337 (1995) 79.